Photothermal-Responsive Single-Walled Carbon Nanotube-Based Ultrathin Membranes for On/Off Switchable Separation of Oil-in-Water Nanoemulsions

Liang Hu,[†,‡] Shoujian Gao,[†,‡] Xianguang Ding,[‡] Dong Wang,[†,‡] Jiang Jiang,[‡] Jian Jin,[*,†,‡] and Lei Jiang[§]

[†]Nano-Bionics Division and [‡]*i*-LAB, Suzhou Institute of Nano-Tech and Nano-Bionics, Chinese Academy of Sciences, Suzhou 215123, People's Republic of China and [§]Beijing National Laboratory for Molecular Sciences (BNLMS), Key Laboratory of Organic Solids, Institute of Chemistry, Chinese Academy of Sciences, Beijing 100190, People's Republic of China

ABSTRACT Oil-contaminated wastewater threatens our environment and health, especially that stabilized by surfactants. Conventional separation protocols become invalid for those surfactant-stabilized nanoemulsions due to their nanometer-sized droplets and extremely high stability. In this paper, photothermal-responsive ultrathin Au nanorods/poly(*N*-isopropylacrylamide-*co*-acrylamide) cohybrid single-walled carbon nanotube (SWCNT) nanoporous membranes are constructed. Such membranes are capable of separating oil-in-water nanoemulsions with a maximum flux up to 35 890 $m^2 \cdot h^{-1} \cdot bar^{-1}$ because they feature hydrophilicity, underwater oleophobicity, and nanometer pore sizes. It is remarkable that the permeation flux can be simply modulated by light illumination during the process of separation, due to the incorporation of thermal-responsive copolymers and Au nanorods. Meanwhile, it shows ultrahigh separation efficiency (>99.99%) and desired antifouling and recyclability properties. We anticipate that our ultrathin photothermal-responsive SWCNT-based membranes provide potential for the generation of point-of-use water treatment devices.

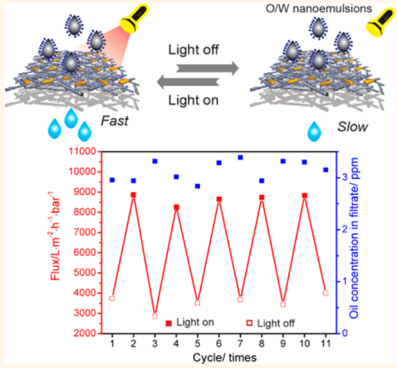

KEYWORDS: photothermal responsivity · ultrathin membrane · oil-in-water nanoemulsion · light-modulated flux · emulsion separation

Water pollution threatens our environment and health, especially oil-contaminated wastewater.[1] Among them, emulsified nanometer-sized oil/water mixtures, or nanoemulsions (particle size: 2−200 nm), are often encountered in petrochemistry, food, and pesticide industries and are highly stable.[2] Traditional separation protocols, such as gravity separation,[3] conventional coagulation,[4] electroflotation,[5] and others,[6] are capable of separating immiscible oil/water mixtures, but they fail to separate nanoemulsions. Moreover, these protocols involve high energy consumption, maintenance expense, and skilled manipulators.[3] Pressure-driven filtration membranes show potential for the disposal of various emulsions,[7−9] but a trade-off between flux and selectivity and severe fouling limits their applications.[7] To solve these obstacles, a myriad of membranes with special wettability have been explored to dispose oil/water mixtures.[10−21] Some nanometer scale porous (or nanoporous) membranes with special wettability have been explored for separation of water-in-oil (W/O) nanoemulsions;[10−12] however, few of them are valid for oil-in-water (O/W) nanoemulsions.[11]

It seems inevitable that nanoporous membranes suffer from low permeation flow due to a small effective pore radius, according to the Hagen−Poiseuille equation, $J = \varepsilon r^2 \Delta p / 8 \mu L$ (where J is the flux of liquid passing through the membrane, ε is the surface porosity, r is the effective pore radius, Δp is the pressure, μ is the liquid viscosity, and L is the thickness of the

* Address correspondence to jjin2009@sinano.ac.cn.

Received for review November 3, 2014 and accepted April 23, 2015.

Published online April 23, 2015
10.1021/nn5062854

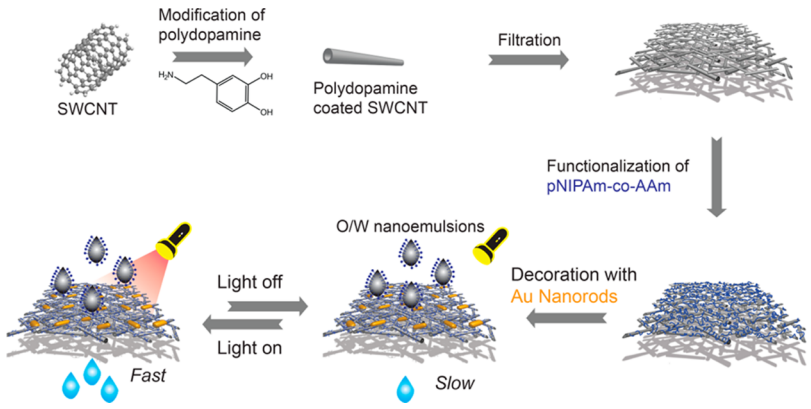

Figure 1. Schematic illustration for the fabrication of photothermal-responsive Au nanorods/pNIPAm-*co*-AAm cohybrid SWCNT ultrathin membranes.

membrane).[22] As a result, ideal membranes which feature an ultrathin selective separation layer and retain its effective pore size are favorable. Unfortunately, it is extremely difficult to construct such structures in traditional filtration membranes, where the contradiction between small thickness and membrane strength is the principal issue.

In this paper, we report a novel approach to construct Au nanorod (ANR)/poly(*N*-isopropylacrylamide-*co*-acrylamide) (pNIPAm-*co*-AAm) cohybrid ultrathin single-walled carbon nanotube (SWCNT) network membranes with light-modulated pore sizes for on/off switchable ultrafast separation of O/W nanoemulsions. This is an important extension of our previous paper in which we reported a new technology for constructing SWCNT membranes, and it could only be effective at separating W/O emulsions due to its hydrophobic and superoleophilic surface wetting properties.[10] Herein, the incorporation of pNIPAm-*co*-AAm endows the ultrathin SWCNT network film with a hydrophilic surface and potential antifouling property, which is beneficial for ultrafast separation of O/W nanoemulsions. Notably, pNIPAm-based copolymers provide the membrane with a chemical valve function by reversibly varying the polymers' conformation triggered by heat and thus resulting in a tunable pore radius[23−27] and correspondingly an on/off switchable permeation property. As membrane separation is a nonstop ongoing procedure, achieving thermal response through direct change in the temperature of an oil/water mixture is unaccessible and thus difficult to be implemented in realistic applications. Alternatively, photothermal-responsive nanoporous membranes enable the realization of uninterrupted and remote control of the pore sizes *via* coupled metal nanoparticles.[26,28,29] By virtue of higher light-to-heat efficiency,[30] ANRs herein are anchored in membranes.

In brief, our photothermal-responsive nanoporous membranes were constructed in four steps (Figure 1), involving (1) modification of the SWCNT with dopamine, (2) fabrication and decoration of the polydopamine-coated SWCNT membrane with (3) pNIPAm-*co*-AAm and, subsequently, (4) excess ANRs. To the best of our knowledge, this is the first sample of photothermal-responsive SWCNT-based ultrathin membranes for on/off-switchable, *or* control flow, separation of O/W nanoemulsions. Ultrahigh separation efficiency and desired antifouling and recyclability properties were achieved. This fact potentially extends the utility of our membranes in the generation of point-of-use (POU) water treatment devices.

RESULTS AND DISCUSSION

Since the pioneering work on mussels, polydopamine has been recognized as an omnipotent binder to many surfaces.[31] In our case, polydopamine was generated spontaneously in solution at high temperature, serving as an interlayer between the pNIPAm-*co*-AAm and SWCNT. Similar to previous reports,[32−34] a noncovalent surface chemistry occurs between the catecholamine polymer and SWCNT, as evidenced by Raman analysis in Supporting Information Figure S1. A transmission electron microscopy (TEM) image in Figure 2a shows that a polydopamine layer is deposited on the SWCNT with a thickness of approximately 2.5 nm. Then, we deposited a certain amount of polydopamine-coated SWCNT solution on a porous mixed cellulous ester (MCE, pore size of 0.45 μm, Figure S2) membrane support, fabricating an ultrathin polydopamine-coated SWCNT membrane *via* a vacuum filtration technique (Figure S3). A scanning electron microscopy (SEM) image in Figure 2b reveals that the polydopamine-coated SWCNT membrane has a randomly oriented interpenetrating network structure with nanometer-sized pores. The surface becomes more hydrophilic, while a high porosity (~45%)[10] is preserved (Figure S4).

Aiming to render membranes photothermally responsive, we synthesized pNIPAm-*co*-AAm copolymers and ANRs. First, the polydopamine-coated SWCNT membrane was incubated in a slight basic solution of pNIPAm-*co*-AAm, such that copolymers

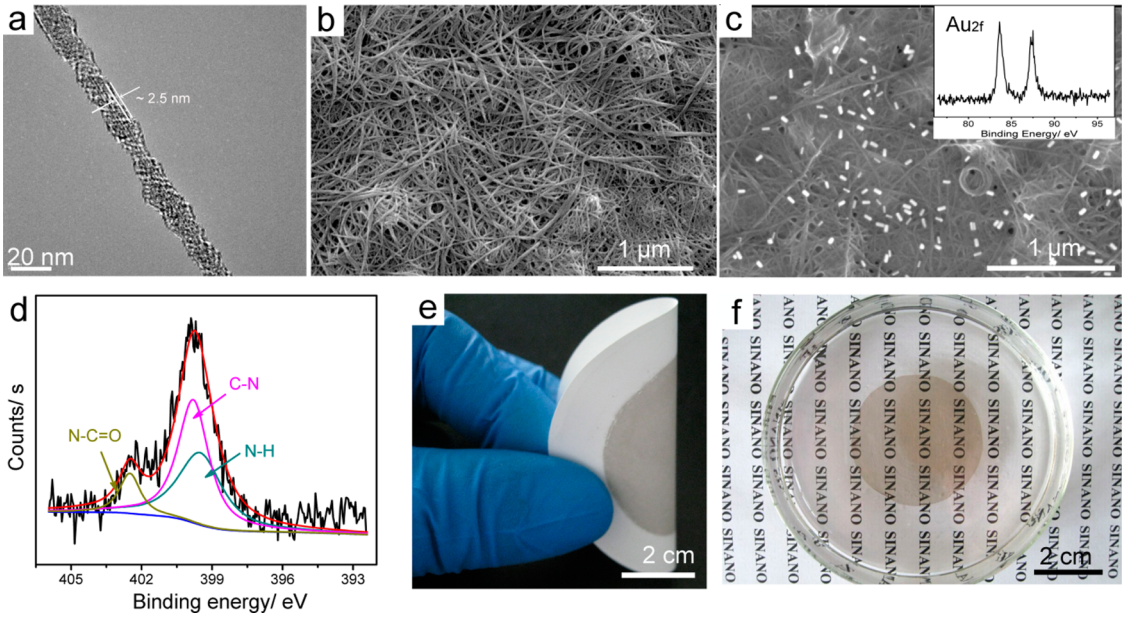

Figure 2. (a) TEM image of polydopamine-coated SWCNT. SEM images of (b) polydopamine-coated SWCNT and (c) ANR/pNIPAm-*co*-AAm cohybrid SWCNT membranes. High-resolution XPS spectra of (inset of c) Au_{2f} and (d) N_{1s} regions for the ANR/pNIPAm-*co*-AAm cohybrid SWCNT membrane. Photographs of the (e) as-prepared and (f) free-standing membrane. The solvent in (f) is acetone.

were anchored to the surface and inside the pores of the membrane by Michael addition.[27] In comparison with NH_2-terminated pNIPAm,[27,35] pNIPAm-*co*-AAm has a lower lower critical solution temperature (LCST), easy preparation, abundant activated sites, and the possibility of postfunctionalization. Next, the pNIPAm-based SWCNT membrane was exposed to a certain amount of ANR dispersions for several hours, where residual NH_2 groups can bind with ANRs.[36] Consequently, ANR/pNIPAm-*co*-AAm cohybrid SWCNT membranes were acquired with a thickness of 77 ± 25 nm (Figure S5). The SEM image and high-resolution X-ray photoelectron spectra (XPS) of the Au_{2f} region in Figures 2c and S6 prove that ANRs are tailored to the surface and do not block the pore of the membrane, thus maintaining a high porosity. In addition to a thin polymer layer (Figure 2c), the other evidence for the introduction of pNIPAm-*co*-AAm can be given by the peak of the XPS N_{1s} signal shifting from 400.2 to 399.8 eV,[37] where the N−C═O signal is located at 402.1 eV (Figures 2d and S6). In a control experiment, we found that ANRs could not be directly attached to polydopamine-coated membranes (Figure S7), again providing sufficient evidence of the presence of the copolymer in the SWCNT membrane. Our ANR/pNIPAm-*co*-AAm cohybrid SWCNT membrane was visually crack-free, homogeneous, mechanically robust, and flexible, and it could be bent more than 100 times while retaining the structural integrity (Figure 2e). Interestingly, a free-standing membrane can be obtained by simply releasing it from the support in anhydrous acetone (Figure 2f), which enables us to transfer the membrane to another chemically inert porous substrate for applications in harsh conditions. Herein, the area of the circular membrane is 12.56 cm^2, but it should be noted that the membrane can be scaled up with ease by using the protocol we described above (data not shown).

Prior to understanding the photothermal responsivity of ANR/pNIPAm-*co*-AAm cohybrid SWCNT membranes, we studied the responsivities of pNIPAm-*co*-AAm and ANRs first. A series of analyses in Figures S8−10 reveal that the obtained pNIPAm-*co*-AAm (M_n = ~38 K, polydispersity = 1.22) contains ~10 mol % of AAm monomer. The thermoresponsivity of pNIPAm-*co*-AAm was investigated using UV−vis spectroscopy with a temperature controller, and the copolymer's LCST is ~38.9 °C, as determined by the "tangent method" (Figure 3a).[38] Accordingly, with the temperature of the solution where the copolymer dissolved is increased across the LCST, and the solution turns opaque. On the other hand, ANRs were synthesized by multiple steps,[39] exhibiting dimensions of 16.1 ± 2.6 nm in diameter and 42.0 ± 4.8 nm in length (averaged from dimensions of 50 random ANRs, Figure 3b). This anisotropic structure yields a longitudinal surface plasmon resonance peak centered at ~627 nm with a full width at half-maximum of 85 nm (Figure S11a), suggesting high monodispersity. Figure 3b displays that the temperature of the ANR solution detected *via* a simple home-designed apparatus (Figure S11b) is increased from 27 to 50 °C within 180 s under laser beam irradiation, while that with DI water is rare. Therefore, it can be concluded that these ANRs exhibit a fast and high photothermal conversion behavior.

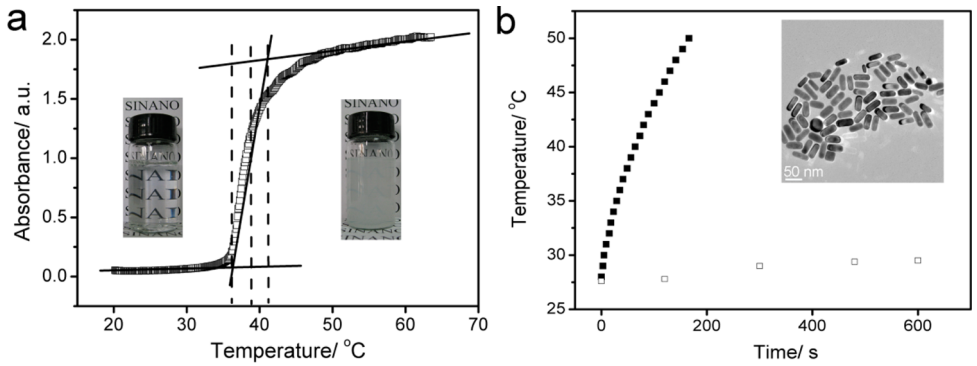

Figure 3. (a) Changes in UV−vis absorbance spectra of pNIPAm-*co*-AAm water solution as a function of temperature where it is dissolved. Insets of (a) are photographs of pNIPAm-*co*-AAm water solution at temperatures (left) lower and (right) higher than LCST. (b) Changes in temperature of the ANR dispersion and DI water as a function of illumination time. Inset of (b) is the TEM image of Au nanorods.

Although the exact mechanism regarding the oil−water emulsion separation membrane is still unclear, we and others feel that it basically involves wettability and a "size-sieving" effect.[10,11,15] For instance, membranes that have the ability to separate O/W nanoemulsions should feature hydrophilicity while the pore sizes are essentially smaller than the size of the emulsion droplets. Therefore, we further examined the surface wettability of the ANR/pNIPAm-*co*-AAm cohybrid SWCNT membrane in response to light irritation *via* measuring the variation of water and underwater oil contact angles. When the laser is turned off, a water droplet (2 μL) displays an initial water contact angle of 56°, and it completely spreads out the membrane after ~2 s (Figure 4a). Nevertheless, when a droplet of dichloroethane (2 μL) contacts the surface underwater, it retains a spherical shape with an oil contact angle of 132°. Such hydrophilic/underwater oleophobic behavior is because water molecules are entrapped into the rough surface, building a new solid/water/oil three-phase system.[40] Water molecules tend to repel dichloroethane, leading to a large oil contact angle. When the dry membrane was exposed under laser irradiation for 8 min, the initial water contact angle increased to 78° (Figure 4b). This is mainly because ANRs absorb and convert light to heat. As heat energy is accumulated and rapidly transfers to the pNIPAm-*co*-AAm *via* the SWCNT matrix (thermal conductivity = 2000 $W \cdot m^{-1} \cdot K^{-1}$),[41] the temperature of the region on the membrane exceeds the copolymer's LCST, resulting in hydrophilicity of the membrane being reduced. Correspondingly, it takes ~4 s for the water droplet to fully permeate into the membrane. In this case, the entrapped water on the surface also does not favor oil spreading and thereby forms an underwater oil contact angle of 134°. These data suggest that our membrane features hydrophilic and underwater oleophobic performance regardless of light exposure. After exposure to light, the enhanced hydrophobicity should have led to a prolonged wetting time; on the contrary, the resultant enlarged pore size, which will be proven later, accelerates the spreading of water droplet on the surface. We therefore suppose that such analogous dynamic wettability can be contributed to the change in the wettability of surface and pores as well as pore size.

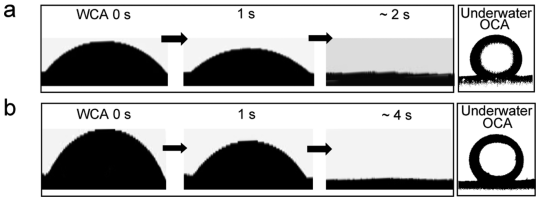

Figure 4. Snapshots of dynamic (left) water and (right) underwater dichloroethane contact angle measurements on the ANR/pNIPAm-*co*-AAm cohybrid SWCNT membrane with light (a) off and (b) on.

We next moved to study how light beams influence the permeation flux, or *J*, using a smaller vacuum filtration system under 0.015 MPa. During the experiments, a random region of membranes (2.54 cm^2) was chosen, and the laser (irradiated area = 1.54 cm^2) was located vertically above the membrane and remained undisturbed during the whole experiment, ensuring all records were obtained in the same manner. We calculated *J* by monitoring the time (*t*) during 5 mL (ΔV) of liquid permeating through the membrane ($J = \Delta V/t$). As shown in Figure 5a, with increasing illumination time, relative flux (J_t/J_0) of the membrane increases to 2.22 ± 0.12, clearly showing that *J* could be systematically tuned as a function of light exposure time. ANRs can convert light to heat energy, which is dissipated by water, thus resulting in an increase in the temperature of the solution (heat capacity of water is 4.18 $kJ \cdot kg^{-1} \cdot K^{-1}$).[28] Meanwhile, ANRs are attached with the copolymer, so this dissipated heat energy indeed leads the copolymer to collapse and thus an increase in *r*. In addition, higher temperature decreases the friction between the membrane and water. In a control experiment, we found that *J* for the pristine SWCNT membrane is increased only 1.12 times from 40 560 ± 1030 to 45 375 ± 1270 $L \cdot m^2 \cdot h^{-1} \cdot bar^{-1}$ under light, which only can be ascribed to the

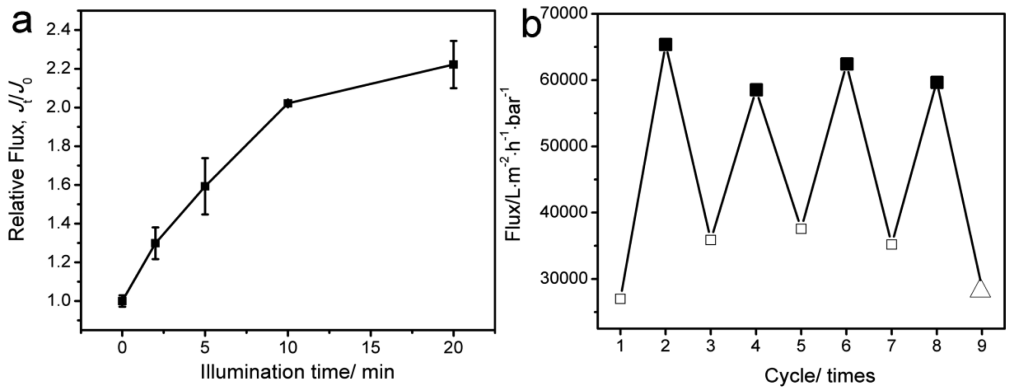

Figure 5. (a) Relative flux changes of the membrane as a function of illumination time. The standard deviations are averaged from three individual experiments. (b) Cycling performance of permeation flux for the membrane with light (■) on/(□) off every 20 min, except for that (△) recorded 1 h after turning the light off.

decreased viscosity of water. As a result, the enhanced J for the cohybrid membrane under light illumination can be mainly due to the change in r. To prove the change in r, we also measured the rejection of the membrane to 13 nm Au nanoparticles. An apparent increase in UV−vis absorbance signals at 525 nm in Figure S12 suggests an expansion of r upon light irradiation. As shown in Figure 5b, such light-modulated J can be realized after multiple light on/off cycles every 20 min without loss of responsivity and repeatability. It also can be seen that J does not drop back to J_0 after 20 min intervals. This is because, when the temperature is decreased, copolymers transition slowly from a collapsed to an extended state, referred to as hysteresis.[42] Accordingly, when the temperature is cooled after ∼1 h, J can be fully recovered. Although a higher J_t/J_0 regarding a pNIPAm-modified porous membrane was reported,[26,27] we want to emphasize that the value of J_t for our membrane is far higher. During the permeation under illumination, heat energy is consumed with water passing through the membrane (thermal conductivity of water is 0.609 $W \cdot m^{-1} \cdot K^{-1}$).[28] As a result, more heat is undoubtedly taken away from the membrane in a certain time, resulting in a lower J_t/J_0. Additionally, amine groups ($-NH_2$) arising from the AAm monomer were anchored to the membrane, probably making the copolymer chains difficult to fully swell/deswell. Also, we think adjusting output wavelength, enlarging light spot size, and/or enhancing output power could offer a higher J_t/J_0, as well.

Given that the ANR/pNIPAm-*co*-AAm cohybrid SWCNT membrane features hydrophilicity, and underwater oleophobicity, as well as tunable nanometer-sized pores, we prepared a series of O/W nanometer-sized emulsions to evaluate its separation capability, including *n*-hexadecane-in-water dodecyl sulfate sodium (SDS)-stabilized nanoemulsion (H/W), isopropyl alcohol-in-water Tween-80-stabilized nanoemulsion (I/W), and chloroform-in-water Tween-80-stabilized nanoemulsion (C/W). The experimental details were similar for the measurements of the water permeation flux. For H/W, it appears semitransparent with a droplet size of 60−460 nm, exhibiting an apparent Tyndall phenomenon (Figure 6a). Once H/W was filtrated through the membrane, a transparent liquid in the filtrate with a drop size of less than 5 nm was collected. This can be explained by the fact that when the H/W emulsion droplet contacts the membrane, *n*-hexadecane is essentially rejected due to the underwater oleophobicity. Combined with the nanometer-sized pore radii, permeation of H/W micelles toward the membrane is hindered. As water passes through the membrane, H/W micelles disassemble simultaneously due to an imbalance of oil/water/emulsifier phases, leaving *n*-hexadecane above the membrane. The droplet size in the filtrate is consistent with the size of SDS micelles in water (Figure S13a), suggesting that a small amount of emulsifier permeated through the membrane during the process. To further test if the membrane could separate the nanoemulsion effectively under illumination, we first noted that H/W was still stable upon laser beam irradiation for 20 min (Figure S13b). As discussed previously, the temperature of the membrane was heated above the LCST of pNIPAm-*co*-AAm after exposure, giving rise to an increase in the effective pore size. Figure 4a shows that H/W can be effectively separated under such conditions, indicating that the increased effective pore size is still far less than the minimum size of the emulsion droplets. Accordingly, J increases from 3670 (J_{off}) to 9000 (J_{on}) $L \cdot m^2 \cdot h^{-1} \cdot bar^{-1}$ (Figure 7), mainly due to enlarged r under light exposure. Total organic carbon (TOC) analysis in Figure 7 clearly shows that the oil concentrations in the filtrate in both cases are less than 5 ppm, which is again possibly due to the amount of emulsifier molecules. We also evaluated the antifouling property of the cohybrid membrane by continuous separation H/W emulsion with multiple light on/off cycles. The calculated J in each case presented in Figure 7 reveals that J upon irradiation is 2.5-fold faster than J_{off}. This J_{on}/J_{off} is larger than that for pure water,

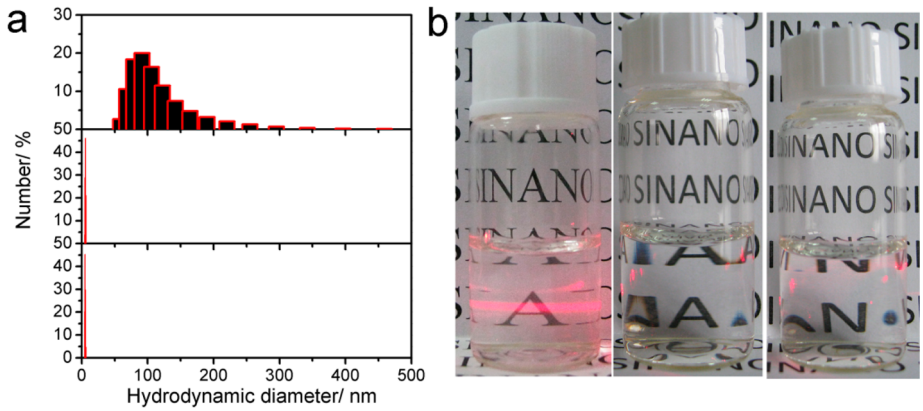

Figure 6. (a) DLS data and (b) corresponding photographs for (top in a, left in b) pristine H/W, filtrate separated under light switched off (middle in a and b) and on (bottom in a, right in b).

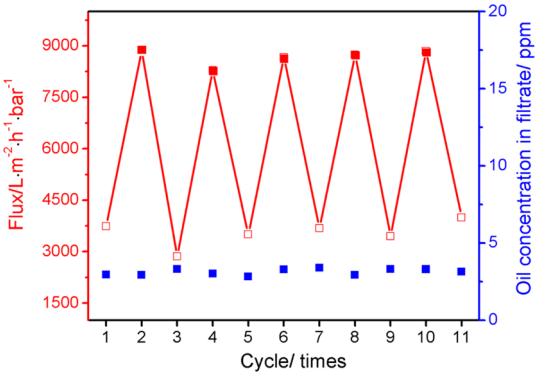

Figure 7. Permeation flux and oil concentration in filtrate for H/W: (open red square) light off and (solid red square) light on.

probably due to the lower heat capacity of *n*-hexadecane (~0.14 $W \cdot m^{-1} \cdot K^{-1}$). Such cycle performance can also be observed multiple times. Importantly, TOC analysis indicates that the purification of the filtrate remains at an ultrahigh level in all cases. In other words, the permeability flow of the membrane can be modulated repeatedly by illumination on/off without any sacrifice of separation efficiency.

As with H/W, I/W (hydrodynamic diameter = 190−820 nm) and C/W (hydrodynamic radius = 5−30 nm) were selected to further verify the feasibility for nanoemulsion separation (Figure S14). Figures S15 and S16 reveal that our membrane can separate both emulsions with illumination switched either on or off, with an oil concentration in the filtrate of <2 ppm. For I/W, the permeate flux of the membrane is significantly increased from 850 ± 20 to 1770 ± 190 $L \cdot m^2 \cdot h^{-1} \cdot bar^{-1}$ under laser beam irradiation. However, both values are lower than those for H/W. Again, water and emulsifiers are allowed to permeate through the membrane during the separation, as evidenced by dynamic light scattering (DLS) analysis for Tween-80 water solution (Figure S15c). We beleive that the increased amount of emulsifiers is a possible reason for the reduced permeate flux. With regard to C/W, Figure S16 shows that the permeate flux of the membrane is surprisingly increased from 11 290 ± 2370 to 35 890 ± 5620 $L \cdot m^2 \cdot h^{-1} \cdot bar^{-1}$, although a barrier layer of chloroform may be created due to its distinct density. Meanwhile, the concentrations of chloroform in filtrate are less than 1.5 ppm. Here, we should mention that the MCE membrane features a substandard polar solvent resistance property. When the MCE membrane is in contact with chloroform, pore sizes of the MCE membrane are enlarged (Figure S16) and influences the permeation flux.[12]

CONCLUSIONS

In conclusion, we have presented a new approach to fabricate photothermal-responsive ultrathin ANR/pNIPAm-*co*-AAm cohybrid SWCNT nanoporous membranes. Due to hydrophilicity, underwater oleophobicity, and nanometer pore sizes, such membranes are intrinsically capable of separating O/W nanoemulsions. Notably, during the process of separation, the permeation flux can be easily modulated by light illumination due to the incorporation of thermal-responsive copolymer and noble metals, while it features ultrahigh separation efficiency and desired antifouling and recyclability properties. *Possibly most importantly*, our ultrathin photothermal-responsive SWCNT-based membranes provide potential for the generation of POU water treatment devices in developing areas.

METHODS

Materials. SWCNTs (o.d. = <2 nm, length = 5−30 μm, purity = >95%) were supplied by Nanjing XFNANO Materials Tech Co., Ltd., China. The MCE filter membrane was commercially available from Beijing Shenghe, China. *N*-Isopropylacrylamide (NIPAm) was provided by TCI (Shanghai, China) and purified by recrystallization from hexane (≥98.5%, Sigma-Aldrich). Ammonium persulfate (APS, ≥98%), sodium borohydride ($NaBH_4$,

≥99%), hexadecyltrimethylammonium bromide (CTAB, ≥99%), sodium dodecyl sulfate (SDS, ≥98.5%), sodium dodecyl benzenesulfonate (SDBS, ≥99%) L-ascorbic acid (Vc, ≥99%), dopamine hydrochloride, and tris(hydroxymethyl)aminomethane (Tris, >99.8%) were obtained from Sigma-Aldrich (Shanghai, China). Hydrogen tetrachloroaurate(III) hydrate ($HAuCl_4$, 99.9%), silver nitrate ($AgNO_3$, >99%), and acrylamide (AAm, >98%) were purchased from Alfa-Aesar (Tianjin, China). Other chemicals were purchased from Sinopharm Chemical reagent Co., Ltd. (China). Deionized (DI) water was produced by a Milli-Q Plus system (Millipore Co.) and showed a resistivity of 18.2 MΩ·cm.

Synthesis of Poly(NIPAm-*co*-AAm) Copolymers. NIPAm (12.6 mmol), AAm (1.43 mmol), and DI water (99 mL) were added to a 250 mL three-neck flask, which was equipped with a reflux condenser, nitrogen inlet, and temperature probe. After the co-monomers were fully dissolved, the solution was purged with N_2 gas and heated to 70 °C. The reaction was initiated with a solution of APS (0.2 mmol) in 1 mL of DI water. The reaction was allowed to react at 70 °C for over 5 h under N_2 gas. Finally, the product was lyophilized using a Scientz-12N (Ningbo scientz biotechology Co. Led) and stored in a plastic tube at 25 °C before use.

Au Nanorod Synthesis. One milliliter of $NaBH_4$ (6 mM) solution was added into a 10 mL mixture of $HAuCl_4$ (0.25 mM) and CTAB (0.1 M). The seed solution was obtained after 2 min under vigorous stirring and aged at room temperature for 30 min prior to use. To prepare the growth solution, 9.0 g of CTAB and 1.1 g of 5-bromosalicylic acid were dissolved in 250 mL of water at 50 °C. After it was allowed to cool at 30 °C for 30 min, 12 mL of $AgNO_3$ (4 mM) solution was injected into the solution, followed by an addition of 250 mL of $HAuCl_4$ solution (1 mM) and, subsequently, 12 mL of ascorbic acid solution (64 mM). Finally, 0.8 mL of seed solution was mixed with the growth solution at 30 °C for 12 h. The reaction products were isolated by centrifugation at 8000 rpm for 10 min followed by removal of the supernatant two times.

Au Nanoparticle Synthesis. Five milliliters of sodium citrate (38.8 mM) was added to a boiling $HAuCl_4$ solution (50 mL, 1 mM). The reaction occurred at higher temperature for 30 min.

Preparation of Polydopamine-Coated SWCNT Membranes. Dopamine (0.1 mg/mL) was added into a Tris-HCl (10 mM, pH = 7.5) solution of SDBS/SWCNTs (0.02 mg/mL). It was allowed to stir at 40 °C for 36 h. Then polydopamine-coated SWCNTs were obtained by centrifugation at 10 000 rpm for 30 min, and it was diluted 2.5×. The final concentration of polydopamine-coated SWCNT dispersion was ∼0.034 mg/mL. Then 2 mL of the dispersion was poured on a porous MCE membrane support to generate polydopamine-coated SWCNT membranes using a vacuum filtration technique.

Preparation of ANR/pNIPAm-*co*-AAm Cohybrid SWCNT Membranes. Polydopamine-coated SWCNT membranes were immersed in a solution of pNIPAm-*co*-AAm (0.5 mg/mL) dissolved in 20 mL of Tris-HCl buffer (pH = 8.5, 10 mM). The reaction was allowed to process at 60 °C for 1 day under shaking, followed by an additional 1 day at 30 °C. After copiously rinsing with DI water, pNIPAm-based SWCNT membranes were dipped into diluted ANR solution and shaken for several hours at 30 °C. Finally, ANR/pNIPAm-*co*-AAm cohybrid single-walled carbon nanotube membranes were rinsed with DI water and stored at room temperature.

Preparation of Oil-in-Water Nanoemulsions. For the *n*-hexadecane-in-water nanoemulsion, *n*-hexadecane (1 mL) was added to the mixture of sodium dodecyl sulfate (0.1 mg, 1×10^{-4} wt %) and DI water (99 mL) under stirring for 1 day. Then, it was diluted 15×. For the iso-octane-in-water nanoemulsion, 20 mL of Tween-80 (14.3 wt %) was dissolved in 80 mL of DI water in the presence of 20 mL of butyl alcohol, followed by an addition of 20 mL of iso-octane. The mixture was stirred for 1 day and diluted 100×. For the chloroform-in-water nanoemulsion, a mixture containing 0.15 g of Tween-80 (0.12 wt %), 120 mL of DI water, and 1 mL of chloroform was stirred for 3 h.

Characterization. ^{1}H nuclear magnetic resonance (^{1}H NMR) was obtained on a Varian 400 MHz, and attenuated total reflectance Fourier transform infrared (ATR FTIR) was performed on Nicolet 6700. UV−vis spectra were obtained on a Lambda 25 UV/vis spectrometer (PerkinElmer) with a thermal controller. Molecular weight (M_w) and molecular weight polydispersity of the copolymer were measured using gel permeation chromatography (GPC, Agilent PL-GPC 50). SEM and TEM images were carried out on field emission scanning electron microscope (Hitachi S4800 japan) and a Tecnai G2 F20 S-twin field emission transmission electron microscope, respectively. The surface element analysis of the membrane was performed on high-resolution X-ray photoelectron spectroscopy (ESCALABMKLL, VG, UK). Atomic force microscopy was conducted using Nanoscope IIId (Veeco Inc. Goleta, CA). Raman spectroscopy was carried out on Labram HR800, Horiba Jobin Yvon, and the excitation wavelength was 532 nm from a He−Ne laser. Contact angles were measured using the sessile drop method (SL200C optical contact angle meter, Solon Information Technology Co). The laser (ADR-1860, beam wavelength = 808 ± 5 nm, beam area at aperture = 1.54 cm^2) was provided by Changchun Feimiao Tech. Led., China. For contact angle measurements, the power was adjusted to 1.22 W/cm^2 in the event that the dry membrane was burned. For photothermal responsivity of ANRs and permeation flux of the membrane measurements, the power was 3.38 W/cm^2. The size of nanoemulsion was measured by dynamic light scattering (Malvern Zen 3600). The oil concentration in the filtrate was measured using a total organic carbon analyzer (Aurora 1030W, USA). Photographs were taken using Canon IXY Digital 8101S.

Conflict of Interest: The authors declare no competing financial interest.

Supporting Information Available: Raman spectra of SWCNT-based membranes; SEM image of a porous MCE membrane before and after contact with chloform and the deposition of ANRs on polydopamine-coated SWCNT membranes; photograph of the vacuum filtration system; SEM image and water contact angle of the SWCNT membrane; water contact angle of the polydopamine-coated SWCNT membrane; AFM image for the cross section of the ANR/pNIPAm-*co*-AAm cohybrid SWCNT membrane; high-resolution XPS spectra of the SWCNT-based membranes; ATR FTIR, ^{1}H NMR, and GPC spectra for pNIPAm-*co*-AAm; UV−vis spectra of the synthesized ANR dispersion, Au nanoparticles, Au nanoparticles in filtrate separated under light on and off; schematic setup for the ANR photothermal conversion experiment; DLS data for SDS micelles in DI water, Tween-80 water solution, H/W upon irradiation for 20 min, I/W, C/W, the filtrate of I/W and H/W separated under light switched off and on; permeation flux and oil concentration in filtrate for I/W and C/W under different conditions. The Supporting Information is available free of charge on the ACS Publications website at DOI: 10.1021/nn5062854.

Acknowledgment. J.J. acknowledges the support from the National Basic Research Program of China (2013CB933000), the National Natural Science Foundation of China (21433012), the Key Development Project of Chinese Academy of Sciences (KJZD-EW-M01-3), and the Natural Science Foundation of Jiangsu Province (BK20130007). L.H. thanks the funding from the National Natural Science Foundation of China (51403231), and the Jiangsu Planned Projects for Postdoctoral Research Funds (1401067C). D.W. thanks the funding from the National Natural Science Foundation of China (21473239).

REFERENCES AND NOTES

1. Shannon, M. A.; Bohn, P. W.; Elimelech, M.; Georgiadis, J. G.; Marinas, B. J.; Mayes, A. M. Science and Technology for Water Purification in the Coming Decades. *Nature* **2008**, *452*, 301–310.
2. Silva, H. D.; Cerqueira, M. A.; Vicente, A. A. Nanoemulsions for Food Applications: Development and Characterization. *Food Bioprocess Technol.* **2012**, *5*, 854–867.
3. Cheryan, M.; Rajagopalan, N. Membrane Processing of Oily Streams. Wastewater Treatment and Waste Reduction. *J. Colloid Interface Sci.* **1998**, *151*, 13–28.
4. Ríos, G.; Pazos, C.; Coca, J. Destabilization of Cutting Oil Emulsions using Inorganic Salts as Coagulants. *Colloids Surf., A* **1998**, *138*, 383–389.

5. Mostefa, N. M.; Tir, M. Coupling Flocculation with Electroflotation for Waste Oil/Water Emulsion Treatment. Optimization of the Operating Conditions. *Desalination* **2004**, *161*, 115–121.
6. Moosai, R.; Dawe, R. A. Gas Attachment of Oil Droplets for Gas Flotation for Oily Wastewater Cleanup. *Sep. Purif. Technol.* **2003**, *33*, 303–314.
7. Lee, S.; Aurelle, Y.; Roques, H. Concentration Polarization, Membrane Fouling and Cleaning in Ultrafiltration of Soluble Oil. *J. Membr. Sci.* **1984**, *19*, 23–38.
8. Lipp, P.; Lee, C. H.; Fane, A. G.; Fell, C. J. D. A Fundamental Study of the Ultrafiltration of Oil–Water Emulsions. *J. Membr. Sci.* **1988**, *36*, 161–177.
9. Pendergast, M. M.; Hoek, E. M. V. A Review of Water Treatment Membrane Nanotechnologies. *Energy Environ. Sci.* **2011**, *4*, 1946–1971.
10. Shi, Z.; Zhang, W.; Zhang, F.; Liu, X.; Wang, D.; Jin, J.; Jiang, L. Ultrafast Separation of Emulsified Oil/Water Mixtures by Ultrathin Free-Standing Single-Walled Carbon Nanotube Network Films. *Adv. Mater.* **2013**, *25*, 2422–2427.
11. Tao, M.; Xue, L.; Liu, F.; Jiang, L. An Intelligent Superwetting PVDF Membrane Showing Switchable Transport Performance for Oil/Water Separation. *Adv. Mater.* **2014**, *26*, 2943–2948.
12. Solomon, B. R.; Hyder, M. N.; Varanasi, K. K. Separating Oil–Water Nanoemulsions Using Flux-Enhanced Hierarchical Membranes. *Sci. Rep.* **2014**, *4*, 5504.
13. Feng, L.; Zhang, Z. Y.; Mai, Z. H.; Ma, Y. M.; Liu, B. Q.; Jiang, L.; Zhu, D. B. A Super-hydrophobic and Super-oleophilic Coating Mesh Film for the Separation of Oil and Water. *Angew. Chem., Int. Ed.* **2004**, *43*, 2012–2014.
14. Gao, X. F.; Xu, L. P.; Xue, Z. X.; Feng, L.; Peng, J. T.; Wen, Y. Q.; Wang, S. T.; Zhang, X. J. Dual-Scaled Porous Nitrocellulose Membranes with Underwater Superoleophobicity for Highly Efficient Oil/Water Separation. *Adv. Mater.* **2014**, *26*, 1771–1775.
15. Yang, H. Y.; Han, Z. J.; Yu, S. F.; Pey, K. L.; Ostrikov, K.; Karnik, R. Carbon Nanotube Membranes with Ultrahigh Specific Adsorption Capacity for Water Desalination and Purification. *Nat. Commun.* **2013**, *4*, 2220.
16. Yang, H. C.; Liao, K.-J.; Huang, H.; Wu, Q. Y.; Wan, L.-S.; Xu, Z.-K. Mussel-Inspired Modification of a Polymer Membrane for Ultra-high Water Permeability and Oil-in-Water Emulsion Separation. *J. Mater. Chem. A* **2014**, *2*, 10225–10230.
17. Tuteja, A.; Choi, W.; Ma, M.; Mabry, J. M.; Mazzella, S. A.; Rutledge, G. C.; McKinley, G. H.; Cohen, R. E. Designing Superoleophobic Surfaces. *Science* **2007**, *318*, 1618–1622.
18. Zhang, L.; Zhang, Z.; Wang, P. Smart Surfaces with Switchable Superoleophilicity and Superoleophobicity in Aqueous Media: Toward Controllable Oil/Water Separation. *NPG Asia Mater.* **2012**, *4*, e8.
19. Zhang, J.; Seeger, S. Polyester Materials with Superwetting Silicone Nanofilaments for Oil/Water Separation and Selective Oil Absorption. *Adv. Funct. Mater.* **2011**, *21*, 4699–4704.
20. Gao, S. J.; Shi, Z.; Zhang, W. B.; Zhang, F.; Jin, J. Photoinduced Superwetting Single-Walled Carbon Nanotube/TiO_2 Ultrathin Network Films for Ultrafast Separation of Oil-in-Water Emulsions. *ACS Nano* **2014**, *8*, 6344–6352.
21. Gao, S. J.; Zhu, Y. Z.; Zhang, F.; Jin, J. Superwetting Polymer-Decorated SWCNT Composite Ultrathin Films for Ultrafast Separation of Oil-in-Water Nanoemulsions. *J. Mater. Chem. A* **2015**, *3*, 2895–2902.
22. Baker, R. W. Overview of Membrane Science and Technology. *Membrane Technology and Applications*, 3rd ed.; Wiley: New York, 2012; p 8.
23. Wu, D.; Liu, X.; Yu, S.; Liu, M.; Gao, C. Modification of Aromatic Polyamide Thin-Film Composite Reverse Osmosis Membranes by Surface Coating of Thermo-responsive Copolymers P(NIPAM-*co*-Am). I: Preparation and Characterization. *J. Membr. Sci.* **2010**, *352*, 76–85.
24. Xie, R.; Li, Y.; Chu, L. Y. Preparation of Thermo-responsive Gating Membranes with Controllable Response Temperature. *J. Membr. Sci.* **2007**, *289*, 76–85.
25. Wang, W.; Tian, X.; Feng, Y.; Cao, B.; Yang, W.; Zhang, L. Thermally On–Off Switching Membranes Prepared by Pore-Filling Poly(*N*-isopropylacrylamide) Hydrogels. *Ind. Eng. Chem. Res.* **2010**, *49*, 1684–1690.
26. Morones-Ramirez, J. R. Bioinspired Synthesis of Optically and Thermally Responsive Nanoporous Membranes. *NPG Asia Mater.* **2013**, *5*, e52.
27. Clodt, J. I.; Filiz, V.; Rangou, S.; Buhr, K.; Abetz, C.; Hoche, D.; Hahn, J.; Jung, A.; Abetz, V. Double Stimuli-Responsive Isoporous Membranes *via* Post-modification of pH-Sensitive Self-Assembled Diblock Copolymer Membranes. *Adv. Funct. Mater.* **2013**, *23*, 731–738.
28. Vanherck, K.; Hermans, S.; Verbiest, T.; Vankelecom, I. Using the Photothermal Effect To Improve Membrane Separations *via* Localized Heating. *J. Mater. Chem.* **2011**, *21*, 6079–6087.
29. Li, Y.; Verbiest, T.; Strobbe, R.; Vankelecom, I. F. J. Improving the Performance of Pervaporation Membranes *via* Localized Heating through Incorporation of Silver Nanoparticles. *J. Mater. Chem. A* **2013**, *1*, 15031–15038.
30. Chen, H.; Shao, L.; Ming, T.; Sun, Z.; Zhao, C.; Yang, B.; Wang, J. Understanding the Photothermal Conversion Efficiency of Gold Nanocrystals. *Small* **2010**, *6*, 2272–2280.
31. Lee, H.; Dellatore, S. M.; Miller, W. M.; Messersmith, P. B. Mussel-Inspired Surface Chemistry for Multifunctional Coatings. *Science* **2007**, *318*, 426–430.
32. Fei, B.; Qian, B.; Yang, Z.; Wang, R.; Liu, W. C.; Mak, C. L.; Xin, J. H. Coating Carbon Nanotubes by Spontaneous Oxidative Polymerization of Dopamine. *Carbon* **2008**, *46*, 1795–1797.
33. Hu, H.; Yu, B.; Ye, Q.; Gu, Y.; Zhou, F. Modification of Carbon Nanotubes with a Nanothin Polydopamine Layer and Polydimethylamino-Ethyl Methacrylate Brushes. *Carbon* **2010**, *48*, 2347–2353.
34. Ryu, S.; Lee, Y.; Hwang, J.-W.; Hong, S.; Kim, C.; Park, T. G.; Lee, H.; Hong, S. H. High-Strength Carbon Nanotube Fibers Fabricated by Infiltration and Curing of Mussel-Inspired Catecholamine Polymer. *Adv. Mater.* **2011**, *23*, 1971–1975.
35. Tripathi, B. P.; Dubey, N. C.; Simon, F.; Stamm, M. Thermo Responsive Ultrafiltration Membranes of Grafted Poly(*N*-isopropyl acrylamide) *via* Polydopamine. *RSC Adv.* **2014**, *4*, 34073–34083.
36. Leff, D. V.; Brandt, L.; Heath, J. R. Synthesis and Characterization of Hydrophobic, Organically-Soluble Gold Nanocrystals Functionalized with Primary Amines. *Langmuir* **1996**, *12*, 4723–4730.
37. Zangmeister, R. A.; Morris, T. A.; Tarlov, M. J. Characterization of Polydopamine Thin Films Deposited at Short Times by Autoxidation of Dopamine. *Langmuir* **2013**, *29*, 8619–8628.
38. Heppner, I. N.; Islam, M. R.; Serpe, M. J. Unexpected Cononsolvency Behavior of Poly(*N*-isopropylacrylamide)-Based Microgels. *Macromol. Rapid Commun.* **2013**, *34*, 1708–1713.
39. Ye, X.; Jin, L.; Caglayan, H.; Chen, J.; Xing, G.; Zheng, C.; Doan-Nguyen, V.; Kang, Y.; Engheta, N.; Kagan, C. R.; et al. Improved Size-Tunable Synthesis of Monodisperse Gold Nanorods through the Use of Aromatic Additives. *ACS Nano* **2012**, *6*, 2804–2817.
40. Liu, M.; Zheng, Y.; Zhai, J.; Jiang, L. Bioinspired Super-antiwetting Interfaces with Special Liquid–Solid Adhesion. *Acc. Chem. Res.* **2009**, *43*, 368–377.
41. Pop, E.; Mann, D.; Wang, Q.; Goodson, K.; Dai, H. Thermal Conductance of an Individual Single-Wall Carbon Nanotube above Room Temperature. *Nano Lett.* **2006**, *6*, 96–100.
42. Hu, L.; Serpe, M. J. Controlling the Response of Color Tunable Poly(*N*-isopropylacrylamide) Microgel-Based Etalons with Hysteresis. *Chem. Commun.* **2013**, *49*, 2649–2651.